Composites Science and Technology 153 (2017) 273–281

Contents lists available at ScienceDirect

Composites Science and Technology

journal homepage: http://www.elsevier.com/locate/compscitech

Particle removal mechanisms in synergistic aging of polymers and glass reinforced polymer composites under combined UV and water

T. Lu, E. Solis-Ramos, Y.B. Yi, M. Kumosa*

National Science Foundation Industry, University Cooperative Research Center for Novel High Voltage/Temperature Materials and Structures, University of Denver, 2155 E Wesley Ave, Denver, CO 80208, USA

ARTICLE INFO

Article history:
Received 20 June 2017
Received in revised form
18 September 2017
Accepted 26 October 2017
Available online 3 November 2017

Keywords:
Synergistic aging
GRP
Hydrodynamic surface effects
Particle removal
Polymers

ABSTRACT

Complex degradation processes occur during synergistic aging of polymers and Polymer Matrix Composites (PMCs) by UV radiation and water condensation at elevated temperatures. The damage is associated with the formation of surface micro-particles and their subsequent removal by slowly moving water. The particle removal significantly accelerates the overall degradation process of the materials [1]. In this research, hydrodynamic effects have been analyzed to explain removals of micro-particles from polymeric materials affected by synergistic aging by UV and water. Viscous shear stresses generated by slowly moving water were determined on polymer surfaces as a function of surface morphology, flow rates, and volumetric forces. Subsequently, a new micro-particle removal mechanism was suggested by comparing the adhesion forces calculated using the Johnson-Kendall-Roberts (JKR) model and the Hamaker approach with the drag forces created by slow water flows. In the experimental part, the particle removal mechanism has been verified on an inclined unidirectional glass/epoxy surface with randomly distributed epoxy particles subjected to a gravitational flow of water. It has been shown that the movement of polymer particles on polymer/composite surfaces depends very strongly on particle sizes, water velocity and surface morphology. The research presented in this study clearly explains why polymer and GRP degradation by UV in the presence of occasional slow water flows is much faster than just by the individual exposure to UV radiation reported in Ref. 1.

1. Introduction

Environmental aging and degradation of polymers and Polymer Matrix Composites (PMCs) is a well-known phenomenon. It affects the above materials when exposed to a variety of environmental conditions [1–8] either individually or in combination. Current research on this topic, however, is usually limited to one individual degradation factor such as UV light, elevated temperature, water diffusion, acid exposure and others [2–5]. Very few studies have concentrated on synergistic aging under multiple degradation conditions [6–9]. One of them has been recently completed on the environmental degradation of a group of unidirectional glass fiber/polymer composites subjected to combined UV, moisture condensation and elevated temperatures as a function of time [1]. Strong synergistic aging effects were observed when six different GRP composites with E-glass and ECR-Glass Fibers embedded in polyester, vinyl ester, epoxy and polyurethane resins were subjected to cyclic UV radiation/water condensation conditions at elevated temperatures (Table 1 [1]). Aging cycles, consisting of 16 h of UV exposure at 80 °C followed by 8 h of water condensation at 60 °C for 1000 h, resulted in a significantly higher rate of aging than under the long term sequential aging by UV for 1000 h at 80 °C followed by water condensation at 60 °C for another 1000 h.

The synergistic combined cyclic aging resulted in noticeable material weight reductions, whereas the sum of the individual exposers to UV and water resulted in clear weight gains (Table 1). The sequential long term individual UV and water aging of the composites was dominated by water absorption by the materials. The UV and water cyclic aging was dominated by the UV damage to the polymers of the composites accelerated by particle removal (cleaning) from the surface of the composites and individual polymers by slowly moving water (see Fig. 1, Ref. [1]). It has also been observed in Ref. [1] that under the combined UV/water condensation conditions the main role of water is to remove the particles generated by UV (Fig. 1(a)) from the composite surfaces and to expose the underlying virgin polymer to

* Corresponding author.
E-mail address: mkumosa@du.edu (M. Kumosa).

https://doi.org/10.1016/j.compscitech.2017.10.028
0266-3538/

Table 1
Total weight changes with standard deviations for six different GRP composites (A-F) tested in Ref. [1] individually under UV for 1000 h at 80 °C followed by water condensation at 60 °C also for 1000 h (Individual Exposures) and under combined 16 h of UV exposure at 80 °C followed by 8 h of water condensation at 60 °C for 1000 h (Cyclic Exposures).

Composites	Sum of Individual Exposures (%)	STD	Cyclic Exposures (%)	STD
A	0.0471	0.0029	−0.1060	0.0314
B	0.0641	0.0131	−0.1030	0.0050
C	0.0038	0.0016	−0.0889	0.0091
D	0.0126	0.0060	−0.0187	0.0040
E	0.0017	0.0028	−0.0760	0.0086
F	0.0734	0.0049	−0.0823	0.0056

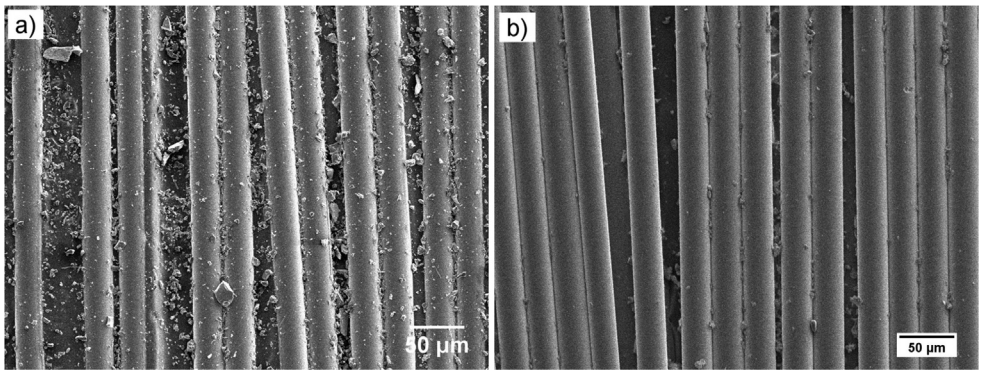

Fig. 1. SEM images of an ECR-glass/epoxy composite after (a) UV radiation for 1000 h at 80 °C and (b) after combined 16 h of UV exposure at 80 °C followed by 8 h of water condensation at 60 °C for 1000 h [1]. The samples were vertically located in a UV chamber and moisture condensation created low velocity water movements on the composite surfaces purely by gravity.

the next UV cycle (Fig. 1(b)).

According to the damage hypothesis made in Ref. [1], the UV/water flow aging model consists of two consecutive stages including: Part (A) UV radiation damage formation on polymer surfaces and Part (B) cleaning UV damage on polymer surface by moving water (Fig. 2). In this research, hydrodynamics effects are added to the degradation study in Ref. [1] to explain in detail the accelerated aging under the cyclic UV/water condensation situation. In particular, the briefly described particle removal model in Ref. [1] is greatly expanded, experimentally verified, and then used to determine the manner micro-polymer particles are moved by slowly moving water on UV damaged polymer and GRP surfaces.

The UV/water synergistic aging model is based on the following main assumptions:

- No water absorption or diffusion occur during condensation exposure.
- Water does not react with the polymer.
- Water flow velocity is low.
- Water is accelerated by the gravity alone.
- The particles are spherical in shape and perfectly smooth.
- The substrate is also perfectly smooth.
- Micro-particles are distributed on the surface as a monolayer and subjected to laminar flows.
- Only adhesion forces between particles and the surface are considered; interactions between particles are neglected.
- Additional less important assumptions will be added to this research.

2. Interaction of particles with substrates

It is known that particle adhesion and detachment depend on many factors such as particle and surface material properties,

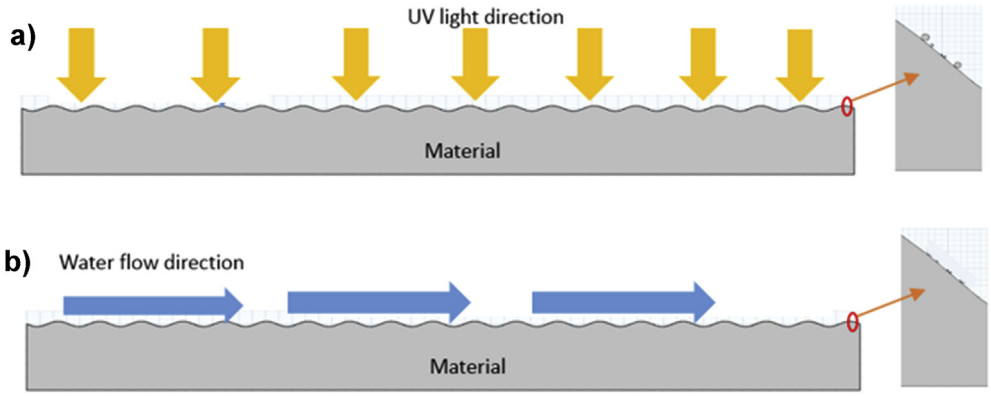

Fig. 2. Material is exposed to the UV radiation (a), then small particles are formed on the surface, which are then washed away by water flow (b).

particle shape and morphology, contact area, and surface roughness [10–12]. To simplify this potentially complicated problem, all of the particles in Ref. [1] and in this work are assumed to be perfectly smooth and spherical. In addition, the effects of gravity and buoyancy are relatively small for micro-scale particles and are neglected [13]. Also, for many microscopic particle systems the electrostatic double layer forces are insignificant compared to the van der Waals forces when the particles and surface are the same material and in contact [14]. Moreover, since the particles are assumed to be constantly immersed in water, capillary forces were also neglected. Therefore, the adhesion forces acting on the particles considered in this research are mainly determined by the Van der Waals forces.

H.C. Hamaker [15] employed the concept of the London-Van der Waals interaction between molecules for the attraction between two spherical macroscopic bodies. If the diameter of one sphere is allowed to approach infinity, the Hamaker equation (Eq. (1)) [13,16,17] can be used for the case of a sphere adhering to a flat surface.

$$F = \frac{A_H d}{12 z_0^2} \tag{1}$$

where F is the adhesion force, A_H is the Hamaker constant, d is the particle diameter, and z_0 is the particle-surface separation distance at contact, which is generally assumed to be the equilibrium spacing in the Lennard - Jones potential equal to 0.4 nm [14,18]. It can be seen, however, that Hamaker's method does not consider the contact area between particles and flat surfaces. To determine the total force including the Van der Waals force and the force acting on the contact area, Eq. (2) has been adapted [19–21].

$$F = \frac{A_H d}{12 z_0^2}\left(1 + \frac{2a^2}{z_0 d}\right) \tag{2}$$

where a is the radius of the contact area between the particle and the flat surface. The contact radius depends on the physical properties of the materials involved. These properties determine whether the particle or the surface will deform, which could be calculated using Eqs. (3)–(6).

Johnson-Kendall-Roberts (JKR) developed a model that included the effect of adhesion forces on the deformation of an elastic sphere in contact with an elastic half space [22]. Accordingly, the contact radius in the model is given in Eq. (3) [21,23,24]:

$$a^3 = \frac{d}{2K}\left[P + \frac{3}{2}W_A \pi d + \sqrt{3\pi W_A d P + \left(\frac{3\pi W_A d}{2}\right)^2}\right] \tag{3}$$

$$W_A = \frac{A_H}{12\pi \cdot z_0^2} \tag{4}$$

$$K = \frac{4}{3}\left[\frac{1-\upsilon_1^2}{E_1} + \frac{1-\upsilon_2^2}{E_2}\right]^{-1} \tag{5}$$

where K is the composite Young's modulus, P is the external force, and W_A is the thermodynamic work [21]. K is given by Eq. (5) in which υ_1 and υ_2, E_1 and E_2 are Poisson's ratios and Young's moduli for the particle and the sample surface, respectively [10,22,23]. In this research, the particles and supporting substrates were assumed to be of the same material; therefore, $\upsilon_1 = \upsilon_2$ and $E_1 = E_2$. The contact radius for a zero external force P in Eq. (2) can be easily derived from Eq. (3), and the simplified result is given by Eq. (6).

$$a = \left(\frac{3\pi W_A d^2}{2K}\right)^{1/3} \tag{6}$$

The Derjaguin-Muller-Toporov (DMT) model [25] is an alternative model for adhesive contact problems which assumes that the contact profile remains the same as in the Hertzian contact but has additional attractive interactions outside the area of contact. According to the DMT model, the contact radius for a zero external force is given in Eq. (7) [26].

$$a = \left(\frac{\pi W_A d^2}{2K}\right)^{1/3} \tag{7}$$

The JKR model is appropriate for soft, highly deformable particles such as soft polymers adhesively bonded to soft surfaces. In case of hard, less deformable particles and substrates, the DMT model should be applied [17,26]. David Tabor [27] showed that the JKR and DMT approaches were the extreme cases of a single theory parameterized by the Tabor coefficient (μ) defined in Eqs. (8) and (9)

$$\mu \sim \left[\frac{R(\Delta\gamma)^2}{K^2 \times z_0^3}\right]^{1/3} \tag{8}$$

$$\Delta\gamma = 2\gamma \tag{9}$$

[28] where R is the radius of the particle, γ is the surface energy of the material, and $\Delta\gamma$ is the work of adhesion. According to Tabor, when the coefficient $\mu \gg 1$, the JKR model should be adapted. However, when the coefficient $\mu \ll 1$, the DMT model should be used [29].

3. Particle removal by hydrodynamics

The characteristic features of photolytic damage is the formation of small micro-size particles on the surface of a glass fiber/polymer composite (Fig. 1(a)). Under combined UV/water flow conditions, these micro-size particles are subsequently removed by the flowing water (Fig. 1(b)) [1]. Here, we assume that the drag force (i.e. viscous shear stress) caused by water flow plays a primary role in the particle removal process. When the viscous shear stress is sufficiently large, UV generated micro-particles will be removed from the surface and expose a fresh undamaged layer to the next UV cycle. According to [20,21], when a stream of fluid passes over a surface with distributed particles, drag forces, lift forces, and external moments of surface stresses are generated. These forces are dependent on the flow conditions, particle conditions and the conditions of the substrate. In this work, Surface roughness is neglected to simplify the model.

Based on [20], there are three potential particle removal mechanisms by water flow: lifting, sliding, and rolling; as shown in Fig. 3. The criteria for particle removal by the mechanisms are derived from the equilibrium equations; see Eqs. (10)–(12). The lifting criterion is derived from the force balance in the vertical direction through Eq. (10). The sliding criterion is derived from the force balance in the horizontal direction according to Eq. (11). The rolling criterion is derived from the moment balance described by Eq. (12).

$$F_l \geq F_a \tag{10}$$

$$F_d \geq u_s(F_a - F_l) \tag{11}$$

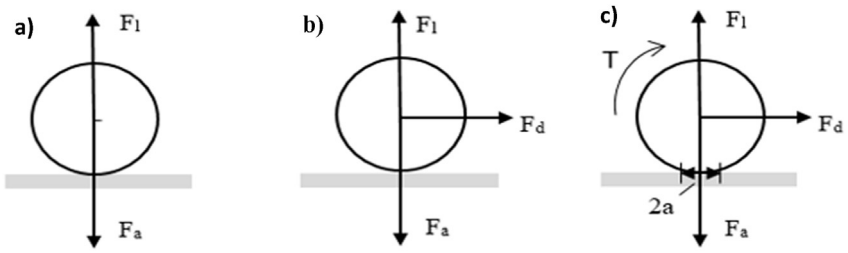

Fig. 3. Particle removal mechanisms in laminar flow: (a) lifting; (b) sliding; and (c) rolling.

$$T + F_l \times a + F_d \times \frac{d}{2} \geq F_a \times a \tag{12}$$

where u_s is the coefficient of wet friction, which was assumed to be 0.01. $\boldsymbol{T}$ is the hydrodynamic moment, F_l is the lifting force, F_d is the drag force, F_a is the adhesion force, a is the contact radius of a particle, and d is the diameter of a particle.

The viscous shear stresses resulting from a pressure difference across the particles are evaluated in this study numerically using COMSOL [30]. The lift forces resulting from a gradient in the shear flow are given in Eq. (13) [31].

$$F_l = 81.2(d/2)^3 \frac{1}{\sqrt{\mu \upsilon}} \tau^{3/2} \tag{13}$$

where υ is the kinematic viscosity, τ is the shear stress and μ is the dynamic viscosity. Dynamic viscosity, also known as absolute viscosity, is a measure of the fluid internal resistance to flow, while the kinematic viscosity is a ratio of the dynamic viscosity to density, $\upsilon = \mu/\rho$.

The drag forces can be estimated using the viscous shear stress in Eq. (14) [30]. The moment of the surface stresses is given by Eq. (15) [20].

$$F_d = 8.014 d^2 \tau \tag{14}$$

$$T = 0.943993 \cdot 2\pi \mu d^2 V_p \tag{15}$$

where the constant 0.943993 accounts for the effect of the surface on the moment [32,33] and V_p is the fluid velocity at the center of the particle (0.01 m/s).

4. Simulation of hydrodynamic effects on flat and wavy surfaces

In our previous UV/water condensation research [1] the samples were positioned perpendicular to the ground and the water flow was driven solely by gravity. Hence, the velocity of the water flow was slow (0.01 m/s) and the thickness of the water layer on a composite surface was assumed to be 0.5 mm. The dynamic viscosity of water at 25 °C, μ, was taken as 8.9×10^{-4} Pa s and its density, ρ_w, was assumed to equal 1000 kg/m^3. The volumetric force, g, was assumed to be 9.8 m/s^2. The open boundary condition was assumed on the water surface in the numerical simulations using COMSOL.

According to [34] the distribution and the magnitude of viscous shear stress are affected by the surface morphology, flow velocity, and the slope of a surface. Under the same water flow rates and volume forces, the distribution and magnitude of viscous stress will be different when different amplitudes and frequencies of wavy surfaces are assumed. This effect could be important on GRP surfaces with large amounts of surface fibers. For the same frequency in the sine function but different amplitudes, water flow velocities and viscous shear stresses were obtained in Fig. 4 and Fig. 5 for 0 mm, 0.02 mm, and 0.2 mm surface amplitudes.

It can be noticed in Fig. 4 that the flow velocity is slightly affected by the amplitudes of sinusoidal surfaces. The maximum flow velocity on the flat surface in Fig. 4(a) was found to be 0.34 m/s, which then decreased to 0.32 m/s on the rough surface in Fig. 4(c). In addition, the average viscous shear stresses of these three different surfaces (Fig. 5) were found to be 1.87 Pa, 1.59 Pa and 0.55 Pa, respectively. It can also be observed in Fig. 4 that when the amplitude of the wavy surface profile increased from 0 mm to 0.2 mm, the maximum viscous shear stress increased almost three times, the average viscous shear stress decreased three times, and the minimum viscous shear stress decreased from 0.5 Pa to around zero. Therefore, when the surface roughness increases, the average viscous shear stress decreases affecting negatively the efficiency of particle removal.

A steadily decreasing viscous stress on a flat surface and significant oscillations of the viscous stresses on a sinusoidal sample surface can be noticed in Fig. 5. The decrease in the shear stress in Fig. 5(a) was caused by a decrease in the gradient of the velocity of water flow as it gained distance in water flow direction (du/dy is decreasing in Eq. (16)). It can be seen in Fig. 5(b) that there are periodic oscillations in the viscous stresses on the polymer surface caused by the initial surface configuration affecting streamlines. Streamlines are the curves that are instantaneously tangent to the velocity vector of the flow. In Fig. 6(a) the streamlines follow the solid wavy interface in the valley locations. However, in Fig. 6(b), the streamline configuration rapidly changed to closed circles inside the valleys, which was caused by an increase in the roughness of the surface. Clearly, under certain circumstances, surface profiles of a sample can rapidly influence the streamline configuration drastically changing water flow and affecting particle removal.

According to the viscous stress distribution along the interface in Fig. 7, locations can be found with the maximum and minimum viscous stresses, respectively. The bottom of the valley exhibits the maximum viscous shear stresses because of a rapid increase in the shear water velocity (du/dy) (Eq. (16)) caused by a decrease of the path area due to the elevated surface profile at that location (0.24 mm). Similarly, slightly over the peak (0.41 mm), the water shear velocity decreases rapidly because an increase in the flow path area leads to a low-pressure condition which eventually forms a minimum shear stress.

$$\tau = \mu \frac{du}{dy} \tag{16}$$

The effect of the volumetric forces is shown in Fig. 8. The volume force equals the gravity when a sample is positioned perpendicular

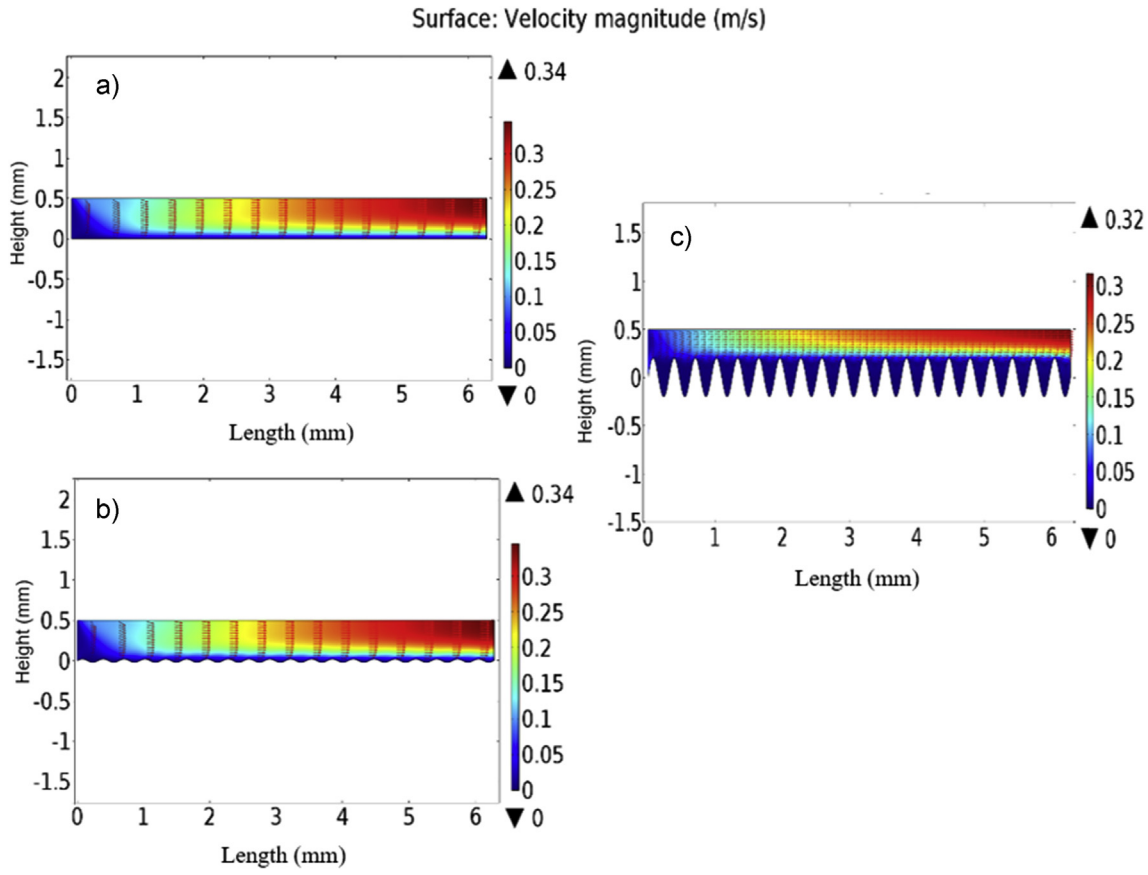

Fig. 4. The effect of surface morphology on water flow velocities for 0 mm, 0.02 mm, and 0.2 mm surface amplitudes all with a frequency of 20 1/s.

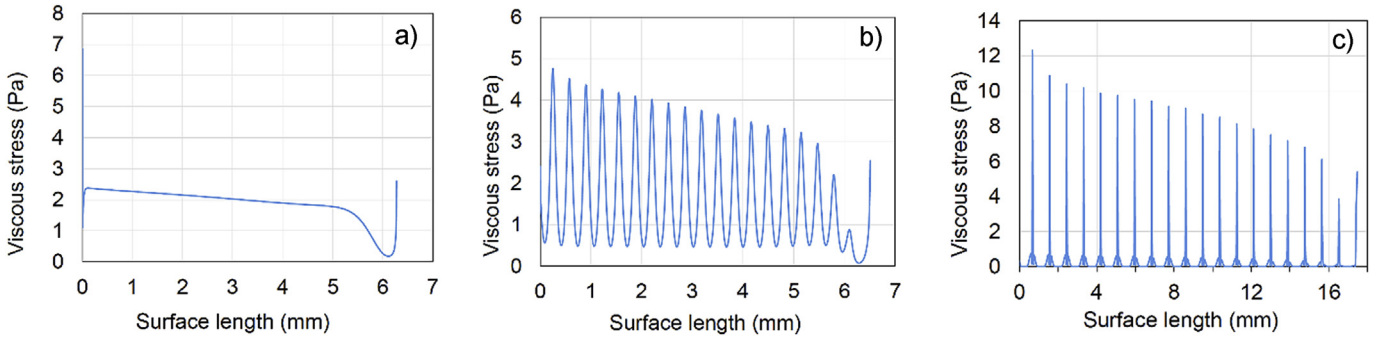

Fig. 5. Viscous stresses along three surfaces with three different surface profiles: flat (a), sinusoid low amplitude (b) and sinusoidal large amplitude (c).

to the ground (90°). However, when the surface is inclined at 45°, the volume force is 0.707 g. Comparing the data in Fig. 8 for the 90° and 45° inclined surfaces, the average shear stresses was reduced from 1.59 Pa to 1.29 Pa, almost a 20% decrease, when the volume forces changes from 1.0 g to 0.707 g.

Correlations between the surface roughness, body forces and viscous stresses are summarized in Fig. 9. Again, when the surface roughness increases, the average viscous shear stress decreases affecting negatively the efficiency of particle removal. Also, when the inclination of the sample surface increases, the average viscous shear stress increases affecting positively the efficiency of particle removal. However, surface roughness (amplitude here) has a more significant effect on particle removal in comparison with surface inclination.

5. Particle removal simulations and preliminary verifications

5.1. Adhesive forces for small epoxy particles on wet epoxy surfaces

According to Section 3, the adhesion forces between smooth spherical micro-particles and a smooth surface are mainly determined by the van der Waals forces. They can be determined using Eqs. (2)–(7) following the DMT and JKR models, and the Hamaker approach. The forces were calculated in this study for epoxy particles assuming that the density of the epoxy, ρ_e, is 1400 kg/m^3, the density of water, ρ_w, is 1000 kg/m^3, the Hamaker constant, A_H, is 1×10^{-20} J [35]; the gap distance, z_0, is 0.4 nm, the Young's modulus of the epoxy, E, is 3.0 GPa, and the Poisson's ratio of the epoxy particles, υ, is 0.38. The surface energy, γ, of the perfectly wet

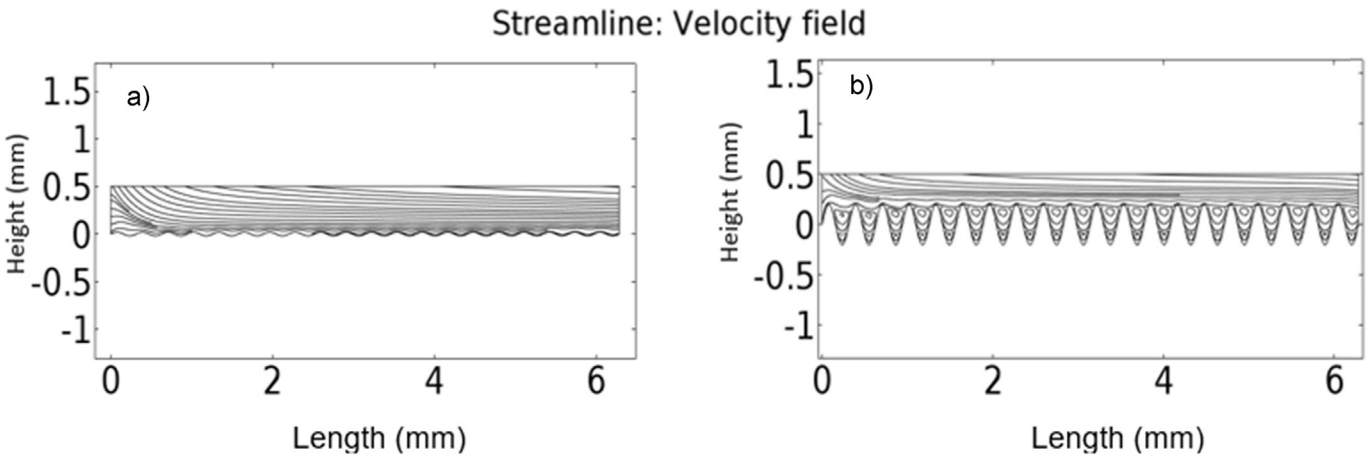

Fig. 6. Streamlines of water flow for 0.02 and 0.2 mm amplitudes.

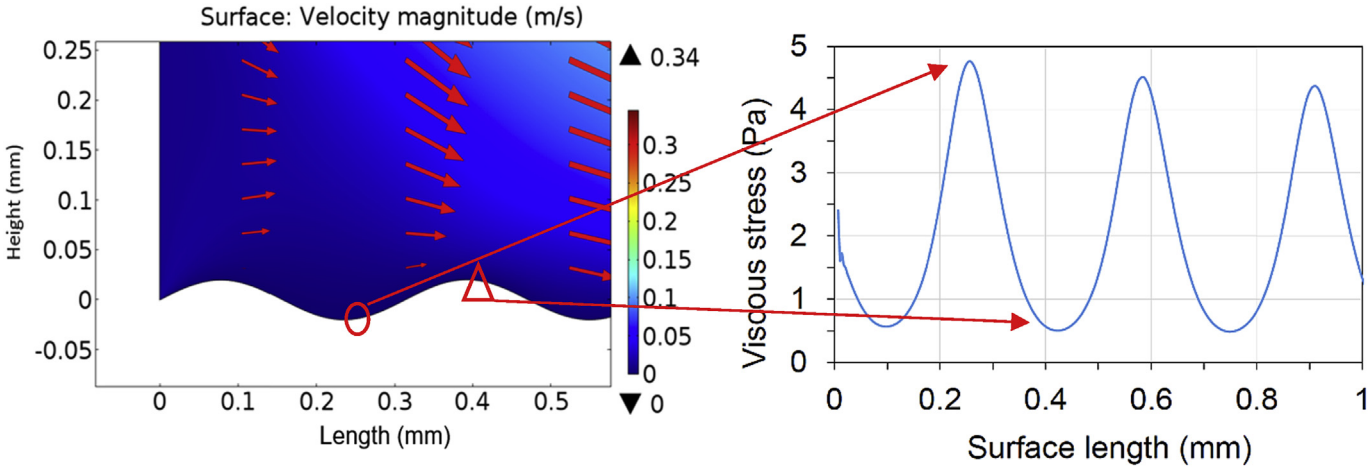

Fig. 7. Maximum and minimum viscous stress locations for 0.02 mm surface amplitudes.

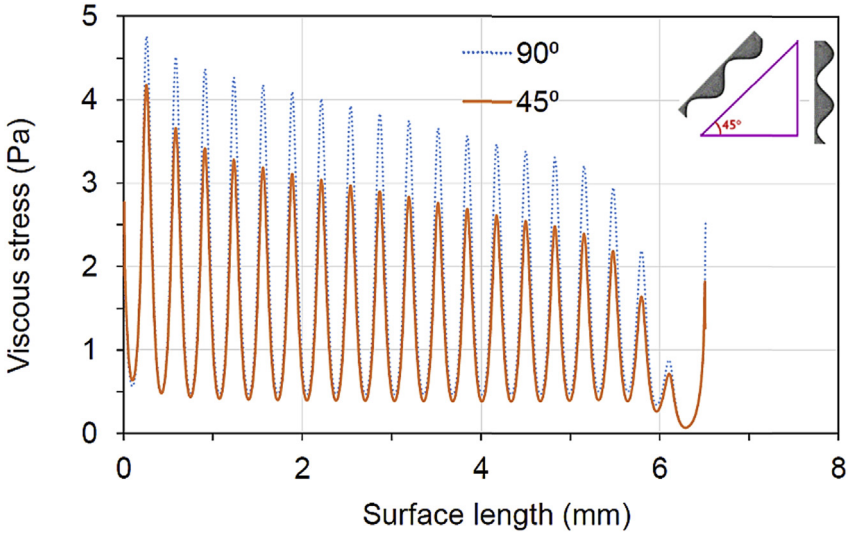

Fig. 8. The effect of volumetric forces on 45° and 90° inclined surfaces.

contact area between the particle and the substrate was assumed to be equal to 0.072 J/m^2 [36]. The estimated van der Waals forces for the assumed physical properties are listed in Table 2 with the estimated weights and buoyancies of the particles.

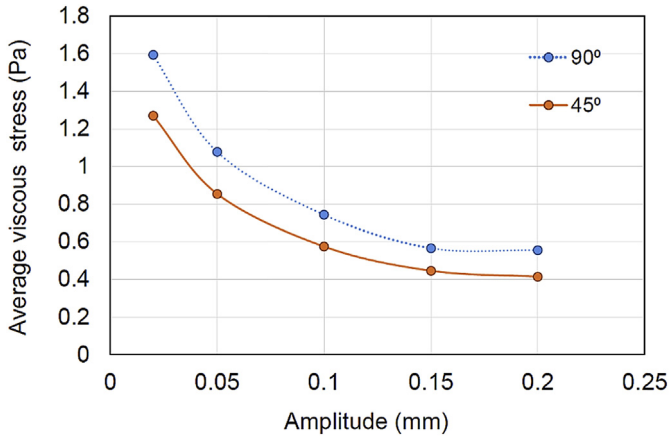

Fig. 9. The effect of surface profile amplitude and surface inclination on average viscous shear stresses.

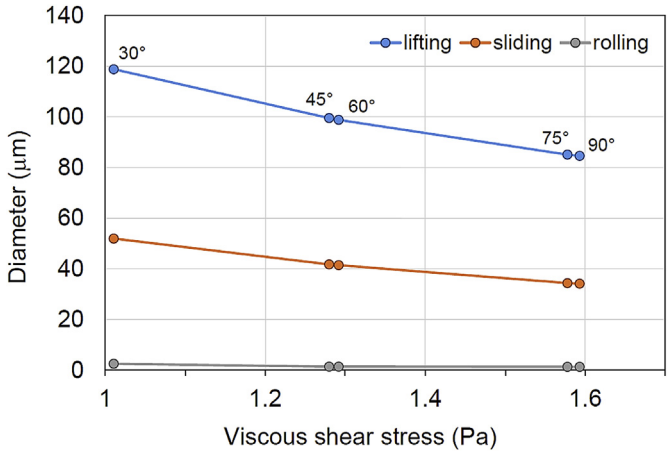

Fig. 10. Critical size of particle which could be removed by different average shear stresses caused by volumetric forces.

It can be seen in Table 2 that the gravitational forces and buoyancies of the particles were much smaller than the van der Waals forces for the particles smaller than 200 μm. Therefore, for small micro size particles their weights and buoyancies could be neglected in the calculation of their adhesion forces. For those particles, the van der Waals force is the main factor which prevents the particle detachment in the presence of water. It can also be observed in Table 2 that the adhesion forces estimated from Eq. (3) by using the contact radii determined from the JKR model are higher than those from the DMT model.

For the assumed physical properties of the particles and the contact area, the Tabor coefficients were subsequently calculated using Eq. (8). The coefficients were found to be ranging from 1.8 to 17 for the particle sizes ranging from 0.2 to 200 μm. According to [29], the JKR model is applicable when the Tabor coefficient is larger than 5. When the Tabor coefficient is around 1, the Maugis-Dugdale model should be adopted [37]. In this study, the JKR method was adopted to calculate the contact radii, which were then substituted into Eq. (2) to calculate the van der Waals adhesion forces [38].

5.2. Explanation of particle removal in Fig. 1 from ref. [1]

For a shear stress of 1.59 Pa obtained from the hydrodynamic FEM model and determined for a surface amplitude of 0.02 mm and by using equations (2)–(15), the movements of the epoxy particles seen in Fig. 1(a) were predicted for gravitational water flows. It has been shown that the particles larger than 1.3 μm can roll, and that the combined sliding/rolling type of motion is possible for particles larger than 34.1 μm. It has also been found that particles larger than 84.5 μm will move by a combination of sliding, rolling and lifting. These preliminary predictions can be verified by the SEM observations in Fig. 1(b). Slow water flows, created by Moisture condensation on vertically positioned composite samples with the fibers oriented with the water flow as shown in Fig. 1, removed almost all the 2-50 μm diameter particles in Fig. 1(b) that were generated by UV radiation in Fig. 1(a). However, smaller particles (<1 μm) still adhered to the surface. This has already been briefly reported in Ref. [1] without however any specifics regarding the combined movements of the particles depending on their sizes.

5.3. Predictions of particle movements on smooth inclined surface caused by moving water

The above simulations were subsequently extended to other shear stresses created by slowly moving water due to gravitational forces on smooth inclined polymer surfaces for the inclination angles of 30°, 45°, 60°, 75° and 90° (Fig. 10). From the particle removal simulations, it is noticed that small particles can be washed away by lifting, sliding or rolling if removal conditions are satisfied. Thus, it is possible for each viscous shear stress in Fig. 10 to remove three different size particles by different combinations of rolling, sliding or lifting mechanisms depending on their diameters. Large size micro-particles will tend to move by the three different movements. On the other hand, smaller particles will tend to mostly roll. Fig. 10 shows these relationships between viscous shear stresses caused by gravitational water flows, particle sizes and their movements on inclined smooth surfaces. It should be stated here that in reality, particle collisions can also have a significant effect on particles' movements. These effects were ignored in this study assuming that each particle is removed independently.

6. Experiment verification of particle removal by hydrodynamic effects

In further validate the particle removal model, an alternative particle removal experiment was designed. A polymeric powder made from crushed epoxy was deposited on a flat glass fiber/epoxy substrate and subjected initially to a constant flow of water of 5 ml/

Table 2
Adhesion and gravitational forces, and buoyancies for epoxy particles of different sizes determined from the DMT and JKR models.

Particle diameter (μm)	Adhesion force (N) DMT	Adhesion force (N)JKR	Gravitational force (N)	Buoyancy (N)
0.2	5.0859×10^{-9}	9.4540×10^{-9}	4.5976×10^{-16}	3.2840×10^{-16}
2	9.7547×10^{-8}	1.9166×10^{-7}	4.5976×10^{-13}	3.2840×10^{-13}
20	1.9813×10^{-6}	4.0088×10^{-6}	4.5976×10^{-10}	3.2840×10^{-10}
200	4.1484×10^{-5}	8.5165×10^{-5}	4.5976×10^{-7}	3.2840×10^{-7}

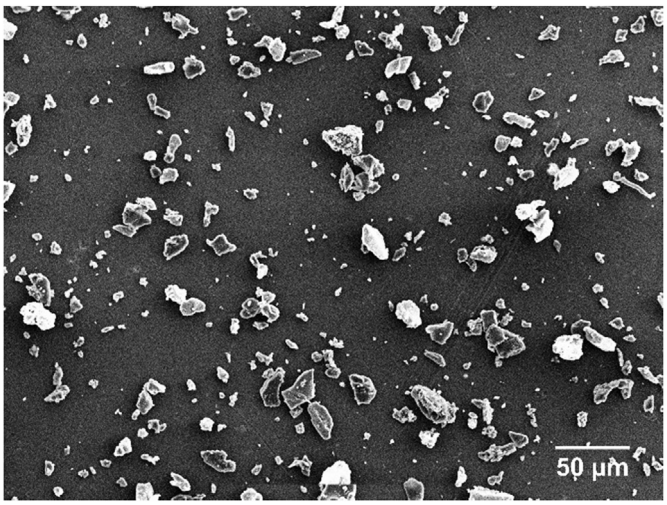

Fig. 11. Initial particle distribution before water cleaning test.

min for 10 min at room temperature. The particle removal efficiency in different areas of the substrate was examined. The initial randomly distributed particles had irregular shapes and were 0.1 and 100 μm in size (Fig. 11). They were distributed inside a region 20 mm by 50 mm, as shown in Fig. 12(a), on an inclined specimen at 30°. After the particle cleaning process was completed, several SEM images were collected from different locations of the substrate to assess the particle interaction with the water flow (Fig. 12(b)).

According to Fig. 5(a), viscous shear stresses decrease along flat surfaces in the direction of water flow. This decrease is caused by a gradient of the water flow velocity. Therefore, any variation in the shear stress would be reflected in the particles' interaction with the flowing water. Based on the water experiment, the extent of particle removal can be estimated to verify the hydrodynamic model simulation. First, from the areas of interest, represented in Fig. 12(b), it can be concluded that the viscous shear stress in location I is larger than that in location II, and the viscous stress in location II is greater than that in location III, as water gains distance,

Table 3
Particle size distribution analyses; maximum Ferret's diameters.

	Initial (before water)	I	II	III
Particle size (μm)	0.1–45	0.1–20	0.1–47	0.1–119
Average size (μm)	8.9	3.5	4.8	9.4

i.e. $\tau_I > \tau_{II} > \tau_{III}$. Secondly, the SEM images in Fig. 13 show that the particle size distribution was different in the selected locations after the water flow. The measurements conducted in those locations are summarized in Table 3.

The small average size of the particles left in region I indicates that most of the large particles were washed away by water, as evident in Fig. 13(I). The largest particles concentrated in region III (Fig. 13 (III)). Therefore, it can be concluded that the viscous shear stress in this location was not large enough to cause significant movements of large particles. Once the large particles began to agglomerate, it is possible that this created an obstacle for the subsequent particles to pass through, which eventually led to the agglomerations of the particles seen in region III. Finally, it can also be observed in Table 3 that the average particle size significantly increases with the water flow direction clearly supporting the hydrodynamic model.

7. Summary observations and conclusions

In this work, hydrodynamics modelling is performed to estimate the viscous shear stresses generated by slowly moving water on polymer and GRP surfaces affected by synergistic aging by UV and water flows. It has been shown that when the surface roughness of the specimens increases, the average viscous shear stress decreases negatively affecting the efficiency of particle removal. On the other hand, when the inclination of the surface increases, the average viscous shear stress increases positively affecting the efficiency of particle removal. A micro-particle removal model is proposed by comparing the adhesion forces calculated by JRK model with the drag forces created by water flows. It has been shown that the movement of polymer particles on polymer surfaces depends strongly on particle sizes, water flow rate, surface morphology, and

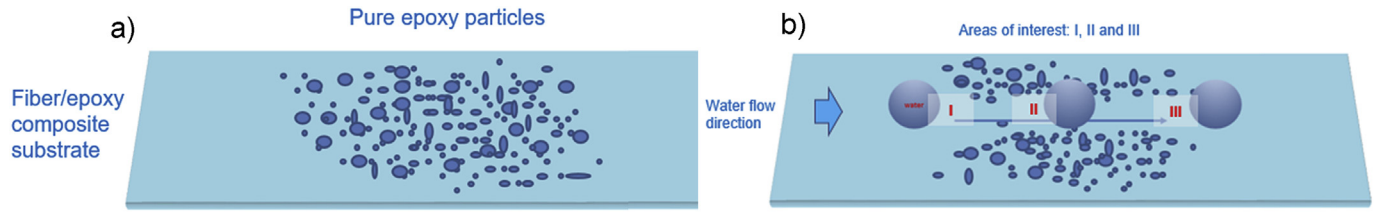

Fig. 12. Schematics of particle distributions (a) before and (b) after water cleaning experiments.

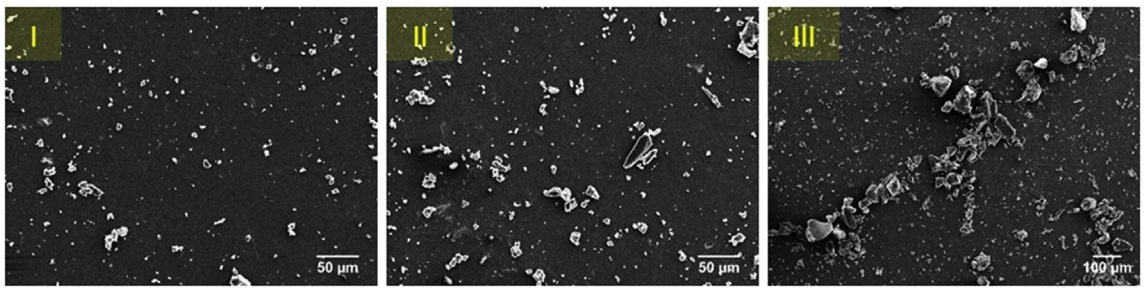

Fig. 13. SEM images of remaining particles after water flow; (I) mostly small particles, (II) combination of small and large particles, and (III) agglomerates of mostly large particles.

the viscous shear stresses caused by the moving water. It was also shown in this research that depending on particle sizes and magnitudes of viscous shear stresses, small particles can be moved by rolling only, and large particles could be cleared by a combination of rolling, sliding and lifting. The particle removal model by water was verified experimentally showing the average size of epoxy particles moved by water on a GRP surface increases in the direction of the water flow.

We have clearly demonstrated in this research that slow water movements caused by rain, mist, moisture condensation and others on polymer and PMC surfaces damaged by UV radiation can accelerate the aging processes by the removal of UV generated polymer micro-particles and by exposing fresh undamaged virgin materials underneath to more UV exposure. The particle removal processes appear to be very complex in nature with complex particle/substrate interactions and particle movements, strongly dependent on many surface conditions and particle sizes.

Acknowledgments

This work was funded by the National Science Foundation I/UCRC Center for Novel High Voltage Materials and Structures under #IIP1362135 and by the NSF Grant Opportunities for Academic Liaison with Industry program under #CMMI-123252.

References

[1] T. Lu, E. Solis-Ramos, Y.B. Yi, M. Kumosa, Synergistic environmental degradation of glass reinforced polymer composites, Polym. Degrad. Stab. 6 (28) (2016) 1–8.
[2] Y. Hu, X. Li, A.W. Lang, Y. Zhang, S.R. Nutt, Water immersion aging of polydicyclopentadiene resin and glass fiber composites, Polym. Degrad. Stab. 124 (2016) 35–42.
[3] J.M. Park, P.S. Shin, Z.J. Wang, D.J. Kwon, J.Y. Choi, S.I. Lee, K.L. DeVries, The change in mechanical and interfacial properties of gf and cf reinforced epoxy composites after aging in NaCl solution, Compos. Sci. Technol. 122 (2016) 59–66.
[4] J. Wang, H. GangaRao, R. Liang, D. Zhou, W. Liu, Y. Fang, Durability of glass fiber-reinforced polymer composites under the combined effects of moisture and sustained loads, J. Reinf. Plastics Compos. 34 (21) (2015) 1739–1754.
[5] P. Böer, L. Holliday, T.H.-K. Kang, Independent environmental effects on durability of fiber-reinforced polymer wraps in civil applications: a review, Constr. Build. Mater. 48 (2013) 360–370.
[6] S. Kiil, Model-based analysis of photoinitiated coating degradation under artificial exposure conditions, J. Coat. Technol. Res. 9 (4) (2012) 375–398.
[7] B.G. Kumar, R.P. Singh, T. Nakamura, Degradation of carbon fiber-reinforced epoxy composites by ultraviolet radiation and condensation, J. Compos. Mater. 36 (2002) 2713–2721.
[8] E. Dionysis, B. Mouzakis, A. Helen Zoga, A.,B. Costas Galiotis, Accelerated environmental ageing study of polyester/glass fiber reinforced composites (GFRPCs), Compos. Part B 39 (2008) 467–475.
[9] E. Solis-Ramos, M. Kumosa, Synergistic effects in stress corrosion cracking of glass reinforced polymer composites, Polym. Degrad. Stab. 136 (2017) 146–157.
[10] G. Iman Goldasteh, A. Monte Carlo, Simulation of micron size spherical particle removal and resuspension from substrate under fluid flows, J. Aerosol Sci. 8 (7) (2013) 62–71.
[11] M.A. Hubbe, Theory of detachment of colloidal particles from flat surfaces exposed to flow, Colloids Surfaces 12 (1984) 151–178.
[12] M. Soltani, G. Ahmadi, On particle adhesion and removal mechanisms in turbulent flows, J. Adhesion Sci. Technol. 8 (7) (1994) 763–785.
[13] M.B. Ranade, Adhesion and removal of fine particles on surfaces, Aerosol Sci. Technol. 7 (2) (1976) 161–176.
[14] J. Visser, Adhesion of colloidal particles, in: E. Matijevic (Ed.), Surface and Colloid Science, John Wiley & Sons, New York, 1976.
[15] H.C. Hamaker, The london-van der Waals attraction between spherical particles, Phys. IV 11 (23) (1937) 1058–1072.
[16] M. Götzinger, W. Peukert, Particle adhesion force distributions on rough surfaces, Langmuir 20 (13) (2004) 5298–5303.
[17] Q. Li, V. Rudolph, W. Peukert, London-van der Waals adhesiveness of rough particles, Powder Technol. 161 (2006) 248–255.
[18] J. Visser, Particle adhesion and removal: a review, Part. Sci. Technol. 13 (1995) 169–196.
[19] G.M. Burdick, N.S. Berman, S.P. Beaudoin, Describing hydrodynamic particle removal from surfaces, Thin Solid Films 488 (2005) 116–123.
[20] G.M. Burdick, N.S. Berman, S.P. Beaudoin, Describing hydrodynamic particle removal from surfaces using the particle reynolds number, Nanoparticle Res. 3 (5) (2001) 455–467.
[21] M.L. Zoeteweij, J.C.J. van der Donck, R. Versluis, Particle removal in linear shear flow: model prediction and experimental validation, Adhes. Sci. Technol. 23 (6) (2009) 899–911.
[22] K.L. Johnson, K. Kendall, A.D. Roberts, Surface energy and the contact of elastic solids, Proc. R. Soc. Lond. A 324 (1971) 301–313.
[23] G. Ahmadi, S. Guo, X. Zhang, Particle adhesion and detachment in turbulent flows including capillary forces, Part. Sci. Technol. 25 (2007) 59–76.
[24] I. Goldasteh, G. Ahmadi, A. Ferro, A model for removal of compact, rough, irregularly shaped particles from surfaces, J. Adhesion 88 (9) (2012) 766–786.
[25] B.V. Derjaguin, V.M. Muller, Y.P. Toporov, On the role of molecular forces in contact deformations (critical remarks concerning dr. Tabor's report), J. Colloid Interface Sci. 67 (2) (1978) 378–379.
[26] X. Zhang, G. Ahmadi, Effects of capillary force and surface deformation on particle removal in turbulent flows, J. Adhesion Sci. Technol. 21 (16) (2007) 1589–1611.
[27] D. Tabor, Surface forces and surface interactions, J. Colloid Interface Sci. 58 (1) (1977) 2–13.
[28] D.E. Packham, Work of adhesion: contact angles and contact mechanics, Int. J. Adhesion Adhesives 16 (2) (1996) 121–128.
[29] A.H.I. Essawey, Microparticle Detachment from Surfaces by Fluid Flow, Doctoral dissertation, University of Notre Dame, Notre Dame, Indiana, January 2004.
[30] Comsol 4.3, COMSOL Multiphysics User's Guide. Burlington, MA.
[31] N. Riefler, M. Heiland, A. Waske, N. Räbiger, S. Odenbach, U. Fritsching, et al., Particle deposition and detachment in capillary sphere packings, Chem. Eng. 174 (1) (2011) 93–101.
[32] M.E. O'Neill, A sphere in contact with a plane wall in a slow linear shear flow, Chem. Eng. Sci. 23 (1968) 1293–1298.
[33] M. Soltani, G. Ahmadi, On particle adhesion and removal mechanisms in turbulent flows, J. Adhesion Sci. Technol. 8 (7) (1994) 763–785.
[34] C. Ozalp, A. Pinarbasi, B. Sahin, Experimental measurement of flow past cavities of different shapes, Exp. Therm. Fluid Sci. 34 (5) (2010) 505–515.
[35] G. Lomboy, S. Sundararajan, K. Wang, S. Subramaniam, A test method for determining adhesion forces and hamaker constants of cementitious materials using atomic force microscopy, Cem. Concr. Res. 41 (2011) 1157–1166.
[36] J.H. Clint, A.C. Wicks, Adhesion under water: surface energy considerations, Int. J. Adhesion Adhesives 21 (4) (2001) 267–273.
[37] K.L. Johnson, Mechanics of adhesion, Tribol. Int. 31 (8) (1998) 413–418.
[38] M. Götzinger, W. Peukert, Particle adhesion force distributions on rough surfaces, Langmuir 20 (13) (2004) 5298–5303.